1   **Iodine speciation and size distribution in ambient aerosols at a coastal new particle formation hotspot of**

2   **China**

3   Huan Yu[1,2], Lili Ren[2], Xiangpeng Huang[2], Mingjie Xie[2], Jun He[3], Hang Xiao[4]

5   1.   Department of Atmospheric Science, School of Environmental Studies, China University of Geosciences,

6   Wuhan 430074, China

7   2.   School of Environmental Science and Engineering, Nanjing University of Information Science and Technology,

8   Nanjing 210044, China

9   3.   Department of Chemical and Environmental Engineering, University of Nottingham Ningbo China, Ningbo

10   315100, China

11   4.   Ningbo Urban Environment Observation and Research Station, Institute of Urban Environment, Chinese

12   Academy of Sciences, Xiamen 361021, China

13   *Correspondence to:* Huan Yu (yuhuan_1981@163.com)

14   **Abstract**

15   Intense new particle formation (NPF) events were observed in the coastal atmosphere during algae growth and

16   farming season at Xiangshan Gulf of east China coast. High nucleation-mode iodine concentrations measured by

17   ultra-performance   liquid   chromatography   coupled   with   quadruple   time-of-flight   mass   spectrometry

18   (UPLC/Q-TOF-MS) confirmed that the NPF events were induced by iodine species. Farmed microalgae, as well as

19   wild algae, could be an important NPF source in coastal areas of China. For the first time, we identified 5 inorganic

20   iodine species, 45 organic iodine compounds (35 molecular formulas) and a group of iodide-organic adducts in

21   ambient aerosols. The concentrations and size distributions of iodine species down to 10 nanometers were

22 measured during the iodine-induced NPF, continental NPF and non-NPF days at the coastal site and compared to

23 those at an inland site. The iodine in the above four types of aerosol samples were characterized by iodate, aromatic

24 iodine compounds, iodoacetic acid/iodopropenoic acid and iodide-organic adducts, respectively. This study sheds

25 light on the iodine sources, formation mechanism and its contribution to the coastal NPF in the context of heavy air

26 pollution in eastern China.

28 **1. Introduction**

29   Iodine is an essential trace element for all mammals (including human being) and some aquatic plants. In the

30 atmosphere, iodine plays an important role in ozone (O_3) depletion, altering HOx and NOx chemistry, mercury

31 oxidation and aerosol formation (Baker et al., 2001; O'Dowd et al., 2002). Marine emission sources of iodine

32 containing species in the atmosphere, such as iodomethane, molecular iodine (I_2), hypoiodous acid (HOI) include

33 marine biota emission (Baker et al., 2000), sea surface iodide (I^-) activation by O_3 (Dixneuf et al., 2009; Mcfiggans

34 et al., 2004; Palmer et al., 2005; Sellegri et al., 2006) and sea surface bubble bursting (Seto and Duce, 1972).

35 Continental iodine sources include soil emission, fossil fuel and biomass combustions and industrial emissions

36 (Redeker et al., 2000; Sive et al., 2007). In recent years, much attention has been paid to the new particle formation

37 (NPF) induced by iodine species (Dall'Osto et al., 2018; Allan et al., 2015; Roscoe et al., 2015; Mahajan et al., 2011;

38 McFiggans et al., 2010; O'Dowd and De Leeuw, 2007; Grose et al., 2007; Yoon et al., 2006; O'Dowd et al., 2002).

39 Based upon current knowledge, a simplified scheme of iodine oxidation and nucleation is described as follows:

40 volatile iodocarbons or I_2 photolyses to I atoms, which react with O_3 to produce IO and IO_2 radicals; subsequently

41 the self-combination of IO and IO_2 forms iodine oxides I_2O_{2-5}; iodine oxoacids HIO_x(x=1-3) were produced either

42 from I_2O_{2-5} hydration or via the reaction of IO and IO_2 reaction with HO_x (Burkholder et al., 2004; Martín et al.,

43   2013; Sipilä et al., 2016); eventually, the clustering of I_2O_{2-5} or HIO_x and the subsequent growth of these ultrafine

44   iodide particles contribute to cloud condensation nuclei (CCN) so as to influence the climate.

45   In the past, iodine concentration or speciation has been measured in natural and drinking water (Chen et al.,

46   2007; Liu et al., 2015; Wang and Jiang, 2008; Wei et al., 2007), precipitation (Gilfedder et al., 2007a; Yoshida et al.,

47   2007), soil (Yoshida et al., 2007), animal and microalgae tissues (Hughes et al., 2006; Kaňa et al., 2015; Shah et al.,

48   2005), edible salts (Yun et al., 2017; Zhang et al., 2010), and milk (Wang and Jiang, 2008). Previous measurements

49   in ambient aerosols showed only three iodine species: I^-, iodate (IO_3^-) and total soluble organic iodine (SOI) and

50   their relative concentration and size distribution varied largely with locations (e.g. inland, coastal or open ocean)

51   (Baker et al., 2001; Gilfedder et al., 2007a, b; Lai et al., 2008; Wimschneider and Heumann, 1995; Xu et al., 2010).

52   The majority of atmospheric models assume that IO_3^- would be the only stable iodine species in aerosols

53   (Saiz-Lopez et al., 2012), because I^- may be eventually oxidized to IO_3^- in aerosols or participate in halogen

54   activation to yield gaseous IX (X=Cl, Br, I). SOI deems to be formed from the reaction of aerosol organic matter

55   with HOI (Baker, 2005b). Organic iodine compounds are more toxic than I^- and IO_3^- to humans (Ding and Zhang,

56   2009) and may play a key role in regulating the recycling of halogens to the gas phase. At present the speciation of

57   organic iodine compounds is the most significant unknowns in aerosol iodine chemistry (Saiz-Lopez et al., 2012).

58   Hence, to study the iodine speciation and size distribution will surely help to understand their sources,

59   transformation mechanisms and deposition rates in the atmosphere.

60   It still poses a challenge to determine organic iodine compounds in ambient aerosol. Up to date, there is no

61   detailed aerosol organic iodine speciation study in the literature. Total SOI was generally calculated as total soluble

62   iodine minus inorganic I^- and IO_3^- (Lai et al., 2008), which can be separated and quantified using an ion

63   chromatography coupled with inductively coupled plasma mass spectrometry (IC-ICP-MS). Although the peaks in

64   IC other than I^- and IO_3^- were suspected to be organic iodine (Gilfedder et al., 2007a, b, 2008), ICP-MS did not

65   provide molecular weight information. Without foreknown information of ion mass, molecular structure or

66   retention time (RT), neither liquid chromatography-MS (LC-MS) nor gas chromatography MS (GC- MS) can be

67   applied to identify and quantify unknown organic iodine in the aerosols. Unlike those in disinfection by-products or

68   iodine-rich seaweed, individual organic iodine compound in a complex aerosol matrix is of extremely low

69   concentration. Based on our experience, organic iodine ions co-elute with many other interfering ions even after

70   chromatographic separation. As a result, it is difficult to apply even high resolution mass spectrometry to identify

71   unknown organic iodine compounds in the aerosols using MS and MS/MS experiments.

72   The populated coastal regions of eastern China are influenced by both industrial and marine emissions.

73   Growing algae population due to serious eutrophication in the coastal waters may promote iodine emission, which

74   make the coastal region a potential hotspot of new particle formation. Up to now, there has been no report of iodine

75   induced NPF in the places out of coastal sites of west Europe (e.g., Mace Head, Ireland; Roscoff, France; O Grove,

76   Spain), Tasmania (Cape Grim) and Polar regions. Besides, the iodine speciation measurement in particles smaller

77   than 100 nm is also scarce (Baker, 2005a; Baker, 2004; Gilfedder et al., 2008; Lai et al., 2008; Wimschneider and

78   Heumann, 1995). The purpose of our study is to characterize iodine speciation using the ultra-performance liquid

79   chromatography coupled with quadruple time-of-flight mass spectrometry (UPLC/Q-TOF-MS) and measure their

80   concentrations in size segregated particles down to 10 nm diameter collected during the NPF events observed at a

81   coastal site of China. The comparison of iodine species between the coastal site and an inland site will also be

82   discussed.

83   **2. Experiments**

84   **2.1 Sampling**

85   A five-month campaign from January to May 2018 was carried out at Xiangshan Gulf of Zhejiang Province on

86   the east coast of China. The coastal observation site (29 °29'N, 121 °46'E, see Figure 1) is a small building about

87   40m and 200m away from the coastline at high tide and low tide, respectively. The Xiangshan Gulf is developed as

88   the largest algae cultivation area of Zhejiang Province. This feature makes the Xiangshan Gulf a potential hotspot

89   of iodine emission from wild or farmed microalgae. We used a scanning mobility particle spectrometer (SMPS) and

90   a Neutral Air Ion Spectrometer (NAIS) to monitor NPF events at the site. The statistical characteristics of new

91   particle formation at the observation site are not the focus of this paper. Instead, a nano Micro-Orifice Uniform

92   Deposit Impactor (nano-MOUDI, MSP Corp, Shoreview, MN) or a median-volume aerosol sampler were used to

93   collect size segregated 10 nm -18 μm aerosols or $PM_{2.5}$ during typical NPF days. The 13-stage nano-MOUDI

94   provides cut sizes of 18, 10, 5.6, 3.2, 1.8, 1.0, 0.56, 0.32, 0.18, 0.10, 0.056, 0.032 and 0.010 μm in aerodynamic

95   diameters when operating at a flow rate of 30 L min^{-1}. Offline method by high resolution mass spectrometer was

96   developed to analyze iodine in the aerosol samples.

97   Particle size distribution from 2 nm to 740 nm was obtained by integrating a long SMPS (TSI DMA3081 and

98   CPC3775; scanning range: 40–750nm) and NAIS (scanning range:2-42nm) data. The SMPS sampled ambient air

99   from a 129cm long and 1.0 cm inner diameter (I.D.) SS tube horizontally oriented with an airflow of 14 standard

100 L min^{-1}. NAIS sampling inlet was a 1.5 m long and 32 cm inner diameter copper tube. The transport loss of

101 particles in the SMPS and NAIS inlets was corrected using size-dependent survival ratios. Scanning cycles of the

102 SMPS and NAIS were synchronized to 4 minutes. The NAIS measured positive ion, negative ion and total particles

103 alternately. Based on the particle size distribution data, we found that unless it was cloudy or rainy, strong NPF

104 events were observed almost every day in April and May, which is the growth and farming season of seaweed. As

105 would be discussed in Section 3, high nucleation-mode iodine concentration suggests these NPF events were

106 induced by iodine (hereafter, I-NPF event). During the cold season without algae farming from January to March,

107 however, only 7 traditional banana-shaped NPF events were observed out of 54 observation days. Given the air

108   mass back trajectories computed by HYSPLIT model (Draxler and Rolph 2003) were from the northwest inland of

109   China, these events were defined as continental NPF.

110   The sampling scheme was implemented based on the above size distribution observations. One set of

111   nano-MOUDI samples was collected during the continental NPF days from February 11 to 13; one set of

112   nano-MOUDI samples was collected during the non-NPF days from April 16 to 18; one set of nano-MOUDI

113   samples was collected during the I-NPF days from May 9 to 11 and three sets of daily $PM_{2.5}$ samples were collected

114   during the I-NPF days from April 25 to 27. Each set of nano-MOUDI samples was collected continuously for 72

115   hours, during which I-NPF or continental NPF occurred on a daily basis, so aerosol chemical composition features

116   of these two types of NPF events can be observed from offline analysis. In addition, as a comparison to the coastal

117   site, four sets of $PM_{2.5}$ samples were randomly collected on January 14, April 15, April 25 and May 5 at an inland

118   urban site 200 km from the coast (see Figure 1). The description of the inland site can be found in Yu et al. (2016).

119   No simultaneous measurement of particle size distribution was made at the inland site.

120   The detailed sampling procedures for $PM_{2.5}$ and nano-MOUDI are as follows. $PM_{2.5}$ aerosols were collected

121   on 90 mm quartz fiber filters using a median-volume aerosol sampler (TH-150C, Wuhan Tianhong Ltd., China) at a

122   flow rate of 100 L min^{-1} for 23 h. Since quartz fiber filters may absorb volatile iodine species like hydrogen iodide

123   (HI), which brings positive artifact to I^{-} measurement in aerosols, a field blank was collected by placing a HEPA

124   filter in the upper stream of a quartz fiber filter. Two nano-MOUDIs were placed side by side to collect 10-100 nm

125   (stages 10-13) and 100 nm-18 μm (stages 1-9) aerosols, respectively. Considering low aerosol mass loading on

126   10-13 stages, the chemical analysis of aerosols collected on 10-13 stages may be sensitive to the particle bounce-off

127   from upper 1-9 stages, Therefore, aluminum foil filters on the 1-9 stages of the first nano-MOUDI were

128   silicon-greased to reduce potential bounce-off artifact on the filters of 10-13 stages that were sent for chemical

129   analysis. For the second nano-MOUDI, all filters were not silicon-greased but only the filters of 1-9 stages were

130   sent for chemical analysis. Before sampling, the filters were baked in a laboratory oven at ca. 500℃ for 24 h to

131   remove organics. After sampling, the filters were packed and stored in a refrigerator below- 20℃.

2.2 Chemical analysis

133   One-fourth or a half of filter was put in a 10 mL amber vial with 1:1 v/v mixture of water (LCMS grade,

134   Aladdin, China) and methanol (LCMS grade, Adamas, China). The filter fraction was sonicated for 40 min and the

135   extract was filtered by a 0.2 μm PTFE membrane syringe filter. The eluate was evaporated to almost dryness in a

136   rotary evaporator below 40℃ and subsequently re-dissolved in 0.5 mL water. After being centrifuged (12000 rpm)

137   for 30 min, the supernatant was collected for MS analysis using a Waters UPLC (BEH column, 1.7 μm column,

138   2.1×50mm) coupled with a Xevo G2 Q-TOF MS. A gradient eluent at flow rate 4mL/min was applied as below:

139   2/98 methanol/water for 0.5 min, linearly increased to 98/2 over 9.5 min, 98/2 held for 2 min, and returned to 2/98

140   for 3 min. The MS was operated in either positive or negative mode with a TOF resolving power of 32000 FWHM

141   (ESI+) or 28000 FWHM (ESI-). The MS was externally calibrated daily in the mass range 50–1200 using a 0.5

142   mM sodium formate solution. A real time Lockmass correction was applied by acquiring leucine-enkephalin

143   spectrum from a lock spray source. Optimized source parameters were as follows: capillary voltage −2.5 kV for

144   ESI- (or +3.0 kv for ESI+), desolvation gas flow 600 L h^{-1} with temperature 450 ^{o}C and source temperature 120 ℃.

145   Depending on the purpose, the QTOF was operated in 3 modes: low energy MS scan mode (in which molecular

146   ions are subject to in-source fragmentation only), high energy MS scan mode (in which molecular ion are subject to

147   both in-source fragmentation and collision induced dissociation) and MSMS mode (in which selected precursor

148   ions are subject to fragmentation with collision induced dissociation before entering TOF). Collision cell voltage

149   scanned from 10 to 40 eV. Mass spectrum was acquired as continuum format and analyzed by the MassLynx 4.1

150   software. The procedure of identification and semi-quantification of iodine species would be explained in detail in

151   Section 3. To validate the semi-quantification by our procedure, 20 samples with relatively high iodine

152   concentration were also analyzed for total soluble iodine using Agilent 7500a ICP-MS (Agilent Technologies,

153   Santa Clara, CA, USA). To do that, 200 µl aerosol extract was diluted to 5 ml for injection and the iodine detection

154   limit of the ICP-MS was 0.1 µg L^{-1}.

155   **3. Result and discussion**

156   Section 3.1 first discusses particle number size distribution patterns of two types of NPF events at the coastal

157   site. Section 3.2 discusses the identification and semi-quantification of iodine species in the ambient aerosols. The

158   speciation and size distribution of iodine species during the two types of NPF events at the coastal site are shown in

159   Section 3.3. The comparison of iodine species between the coastal site and the inland site is discussed in Section

160   3.4.

161   **3.1 Particle number size distribution patterns of iodine-induced NPF and continental NPF events**

162   Figure 2 shows the particle number size distributions during the two NPF types. During the continental NPF

163   events (Figure 2a), the production of 2-7 nm neutral particles began at 8:00~9:00 and ceased at around 15:00. New

164   particle formation appeared to be not associated with the low tide, but followed a nearly identical variation with

165   both solar radiation and daytime tide height. After the formation, new particles grew to about 100~200 nm in the

166   midnight, following a typical banana-shape contour (Figure 2a, 1st row). These features, together with the air mass

167   backward trajectories originated from northwest inland of China, confirm that this was a regional-scale continental

168   NPF event. N_{2-20}, number concentration of 2-20 nm particles, reached up to 7×10^4-1.3×10^5 cm^{-3} during this type of

169   NPF events, which is higher than the average N_{3-20} 2.5×10^4 cm^{-3} during the continental NPF events recorded by us

170   at Nanjing, the inland urban site in 2016 (Dai et al., 2017).

171   On the I-NPF event days, the production of 2-7 nm began at 9:00~10:00 and last until 18:00 (Figure 2b).

172   There is a clear time lag of ~4 hours between solar radiation increase and the production of 2-7 nm. High N_{2-7}

173   (number concentration of 2-7 nm particles) seemed to be associated with low tide during 13:00-15:00. N_{2-20} reached

174   up to 7×10^6 cm^{-3}-1×10^7 cm^{-3}, which is two orders of magnitude higher than those during the continental NPF. The

175   peak N_{2-20} values at this coastal site are also one order of magnitude higher than those recorded during the most

176   intense I-NPF events at Mace Head, Ireland (5×10^5-1×10^6 cm^{-3}) (O'Dowd et al., 2002). Similar to the NPF events

177   observed at Mace Head, a clear nucleation mode below 30 nm was seen on each sampling day and particles rarely

178   grew beyond 30 nm at the coastal site of our study. The "interrupted" growth pattern suggested that the NPF was

179   limited in a relatively small area around the site. Wild and farmed microalgae at the Xiangshan Gulf were likely the

180   source of these high concentration nucleation mode particles. In particular, during the harvesting season, the wet

181   algae have to be dehydrated by exposing them to sunlight for a few days before further processing or transportation.

182   During this process, a large amount of iodine vapors can be emitted and oxidized to produce new particles.

183   It has been reported from both field and laboratory studies that I-NPF is initiated by a pure negative ion

184   nucleation of HIO_3 (Sipilä et al., 2016). We examined neutral, positive and negative nanoparticle concentrations

185   measured by NAIS during the two types of events. It has been found that during the I-NPF events the negative ion

186   concentrations were $100 \pm 102\%$, $8 \pm 13\%$ and $58 \pm 32\%$ higher than those of positive ions in the size ranges of 0.8-2

187   nm, 2-7 nm and 7-20 nm, respectively. On the other hand, negative and positive ion concentrations in all

188   above-mentioned size ranges were almost the same during the continental NPF events (Figure 2a, row 4-6). The

189   neutral particle concentrations during I-NPF events were higher than those in continental NPF events by two orders

190   of magnitude; however, the ion concentrations were similar in both types of NPF events, which were in the

191   concentration range of 100-1000 cm^{-3} in all size bins. As a result, ion/particle ratios were on the order of 10^{-5} (2-7

192   nm) and 10^{-4} (7-20 nm) during the I-NPF events and 10^{-3} (2-7 nm) and 10^{-2} (7-20 nm) during the continental NPF

193   events, suggesting the contribution of ions were negligible in both types of NPF events.

194   **3.2 Iodine speciation and semi-quantification**

195   The high resolution LC-MS offers the prospect of identifying unknown organic compounds in complex

196   samples. Previous studies identified unknown organic iodine compounds in disinfected drinking water and seaweed

197   base on a strategy that the retention time and accurate mass of iodine-containing precursor ions can be selectively

198   determined by searching their product ion I⁻ (m/z 126.9) in MS/MS experiments (Ding et al., 2009; Yang et al.,

199   2016). Unfortunately, their strategy does not work for our aerosol samples because of two difficulties. First, we

200   found that most of iodine-containing ions in our samples were dissociated to release I⁻ due to in-source

201   fragmentation even in the most gentle ionization condition (e.g., low capillary voltage, low source temperature and

202   desolvation temperature). This can been seen from Figure 3(a) that extracted ion chromatograms of m/z 126.9039

203   are of similar intensity in low energy MS scan mode (in-source fragmentation only) and high energy MS scan mode

204   (in-source fragmentation plus collision induced dissociation). In this situation, it is impossible to select

205   unfragmented iodine-containing precursor ions for MSMS experiments. Second, even if organic iodine compounds

206   can survive from in-source fragmentation, there are many co-eluting background interfering ions. It is time and

207   labor consuming to search I⁻ from all co-eluting molecular ions using MSMS experiments. This often becomes

208   impractical because small organic iodine ions and other neighboring ions often appear in the same precursor

209   isolation window of quatrupole.

210   *Iodide-organic adducts*

211   The above in-source fragmentation behavior suggests that a large proportion of iodine-containing substances

212   in our samples are weakly bound iodide-organic adducts. I⁻ is an electronegative weak base, which can bind with

213   hydroxyl, acid or keto groups to form adducts depending upon the polarity and H-bonding capability of

214   organic/inorganic compounds (Lee et al., 2014). This is also the theory that iodide-chemical ionization mass

215   spectrometry (CIMS) uses I⁻ as ionization reagent to measure organics. Our experiment presented in Figure 3b-3d

216   partly supported the above hypothesis. No I⁻ peak was detected after RT 1 min in the extracted m/z 126.9039

217   chromatograms of pure potassium iodide (KI) solution (1 mmol L^{-1}) or an aerosol extract with low concentration of

218   iodine. However, when the aerosol extract was mixed with KI solution for another analysis, elevated I⁻ peaks in low

219   energy MS scan mode (blue line) indicated the formation of iodide-organic adducts. Furthermore, when collision

220   induced dissociation was applied, no additional I⁻ peaks showed up in high energy MS scan mode (red line). Such

221   an observation implies that (1) iodide-organic adducts were formed but easily dissociated in the low energy MS

222   scan mode and (2) no stable organic iodine compounds were formed in the aerosol extract+KI mixture. This is also

223   confirmed by the fact that no new ions were formed by comparing the mass spectra of aerosol extract before and

224   after KI addition. Therefore, all m/z 126.9039 peaks after RT=1 min in a sample by low energy MS scan can be

225   deemed iodide-organic adducts and their total peak area should be proportional to the total concentration of the

226   adducts.

227   ***Organic iodine compounds***

228   On the other hand, the identities of those stable organic iodine compounds, i.e., the compounds with C-I bond

229   that are not or partially dissociated in the ESI source, are still unknown but their atmospheric chemistry may be of

230   more interest. To bypass the difficulty as discussed above, a signal amplification approach has been applied in this

231   study to identify these unknown organic iodine compounds, for which the detailed steps are shown in Figure 4. The

232   approach is analogous to searching a secondary organic aerosol (SOA) tracer in ambient aerosols after its identity

233   as VOC oxidation product is confirmed by smog chamber simulation. A portion of aerosol extract+KI mixture was

234   added with H_2O_2 solution (10 mmol L^{-1}). After reaction for 4 h, the mixture was injected for low and high energy

235   MS scans. As compared to the chromatograms of the untreated mixture (Figure 3d), a considerable amount of stable

236   organic iodine compounds were formed but dissociated only in high energy MS scan (red curve in Figure 3e), in

237   addition to the formation of more iodide-organic adducts (low energy MS scan, blue curve in Figure 3e). These

238   organic iodine compounds are believed to form from the reactions between aerosol organics and HOI that is

239   produced via $H_2O_2 + I^-$ reaction.

240   The identities of these organic iodine compounds can be obtained by comparing MS scan mass spectra (low

241   energy) before and after the H_2O_2 addition using mass defect (MD) *vs.* m/z diagram. The mass spectrum was

242   reconstructed by integrating over RT 0-15 min. All ions above background intensity of 10^4 are shown in Figure 5 as

243   dots and circles stand for the samples before and after H_2O_2 addition, respectively. Benefiting from the large

244   negative mass defect of iodine (0.0961), the negative mass defects of organic iodine compounds are in the range of

245   -0.3~0, which makes them easy to be distinguished from non-iodine containing ions. Therefore, each red circle

246   without a black dot in -0.3~0 mass defect regime in Figure 5 should stand for an organic iodine compound. These

247   potential organic iodine ions were further selected for MSMS experiments to confirm their fragments contained I^-.

248   Four typical aerosol samples collected at the inland site and coastal site were treated using H_2O_2 and O_3 solutions,

249   respectively, and analyzed using MD *vs.* m/z diagrams in both ESI+ and ESI- modes (Step 1, Figure 4). Since mass

250   assignment is more accurate for an amplified symmetrical peak than a small shoulder peak, the amplification of

251   organic iodine compound concentrations helps to obtain accurate masses of potential iodine organic compounds in

252   ambient aerosols. After that, their retention time information in the UPLC was acquired by extracting their ion

253   chromatograms from low energy MS scan data.

254   In step 2, the elemental compositions of organic iodine compounds were calculated from the accurate masses

255   within 1 mDa mass tolerance allowing the elements C, H, N, O, S and I and confirmed by their isotope patterns.

256   The correctness of calculated molecular formulas was further restricted by the matching of at least one sound

257   structure in ChemSpider database. Consequently, a total of 80 formulas (57 in negative mode and 23 in positive

258   mode) were obtained, each of which should represent an organic iodine compound and its isomers. Because both

259   H_2O_2 and O_3 are important oxidants in atmospheric aerosols, the organic iodine compounds formed in Step 1 may

260   also exist in real aerosol samples via the same reaction mechanism in the atmosphere. Therefore, in Step 3 these

261   newly identified 80 formulas were searched in real aerosol samples using a targeted screening strategy based on

262   their accurate mass and retention time. At last, 35 organic iodine formulas were detected, at least once, in our

263   aerosol samples (Table 1). The other formulas were not detected in any of the aerosol samples, probably due to

264   their slower production rate or the absence of corresponding organic precursors in the atmosphere. The number of

265   isomers listed in the second column of Table 1 is based on the number of ion chromatographic peaks observed for

266   given m/z values in the real aerosol samples. The total 45 isomer peaks, as well as their retention times, are shown

267   in Figure S1. Hence, there are in total 45 organic iodine compounds detected in our samples.

268   As shown in Table 1, 35 molecular formulas were classified into four groups: 5 non-aromatic formulas and 30

269   aromatic formulas including 16 CHOI formulas, 3 CHNI formulas and 11 CHONI formulas. The 5 non-aromatic

270   formulas are assigned to iodoacetic acid, diiodoacetic acid, iodopropenoic acid, iodomethanesulfonic acid and

271   diiodomethane. The first 4 compounds are electrophilic substitution products of alpha-H of organic acids by I^+ from

272   HOI or I_2. Diiodomethane is probably from gas-particle partitioning or the product of iodoform reaction of methyl

273   ketones. Iodoacetic acid was identified in 9 of 10 samples collected from the coastal and inland sites. Other 4

274   compounds, however, were mostly found at the coastal site.

275   30 CHOI, CHONI and CHNI formulas are assigned to aromatic compounds that are prone to electrophilic

276   substitution by I^+. The formulas observed in ESI- mode are expected to have a carboxyl or phenol group, while

277   those observed in ESI+ mode should be aromatic or heterocyclic amines. 16 CHOI formulas are iodinated phenols,

278   substituted benzoic acids or phenolic acids. The 3 most frequently detected formulas are $C_8H_7O_2I$, $C_7H_5O_4I$,

279    $C_7H_5O_2I$. CHONI formulas with 3-5 O atoms detected in ESI- mode are iodinated nitrophenol, nitronaphthol or

280   nitrobenzoic acid. CHONI formulas with 1 O atom detected in ESI+ mode are iodinated hydroxyaniline, pyridinol,

281   or quinolinol. The most frequently detected CHONI compounds are $C_6H_4NO_4I$, $C_{10}H_6NO_3I$ and $C_6H_4NO_3I$. CHNI

282   formulas are heterocyclic amines (i.e., pyrazoles, imidazoles and triazoles), among which $C_7H_{11}N_2I$ was detected in

283   4 out of 10 samples.

284   Further assignment of the exact identity for the above formulas is impractical, because these 35 molecular

285   formulas probably stand for hundreds of isomers, for most of which no commercial standards are available.

286   Nevertheless, the identities of 4 compounds have been confirmed including iodoacetic acid ($C_2H_3O_2I$),

287   3-iodo-2-propenoic acid ($C_3H_3O_2I$), 3-iodo-benzoic acid ($C_7H_5O_2I$) and 2-hydroxy-5-iodopyridine (C_5H_4NOI)

288   according to the retention times of their commercial standards. These 4 compounds are identifiable because they

289   have no or very few isomers, of which the commercial standards can be procured. Subsequently, these four

290   compounds can be used as surrogate standards to semi-quantify the concentrations of other organic iodine species.

291   *Inorganic iodine species*

292   In addition to the above organic iodine compounds, some inorganic iodine species were also detected. Figure 6

293   shows the integrated mass spectrum of molecular ions between RT 0.5-0.7 min obtained by low energy MS scan of

294   an S13 nano-MOUDI sample (10-18 nm particles) collected during the I-NPF days. The most abundant species is

295   IO_3^-, followed by I^- and HSO_4^-. I_3^- was also observed, probably due to the adduct formation between I^- and I_2. IO_2^-

296   and IO^- are detectable, but their abundances are two orders of magnitude lower than IO_3^-. Iodine oxides I_2O_{2-5} were

297   not ionizable by the ESI source, but they might have been hydrated to HIO_x and detected as IO_x^- (Sipilä et al. 2016).

298   Iodide-metal complexes like CuI_2^-, $Cu_2I_3^-$, ZnI_3^- and $CuI_2(HCN)(HCl)^-$ were observed in $PM_{2.5}$ samples but not in

299   size-segregated nano-MOUDI samples. Cu^+ and Zn^{2+} are typical coarse model components. The observation thus

300   indicated that the iodide-metal complexes detected in the $PM_{2.5}$ samples were formed only after fine- and

301   coarse-mode components were mixed in the sample extract. To avoid artificial formation of iodide-metal

302   complexes during the sample extraction process, our result highlights the importance of collecting size-segregated

303   samples instead of $PM_{2.5}$ or PM_{10}.

304   *Semi-quantification of identified iodine species*

305   So far 35 organic iodine formulas (45 isomer peaks) and 5 inorganic iodine anions have been identified. In

306   order to know their size distributions and relative abundances in different types of samples, the following strategy

307   was applied to semi-quantify these iodine species (step 4, Figure 4): external calibration curves of peak area *vs.*

308   concentration were established by analyzing standard solutions of KI, KIO_3, iodoacetic acid, 3-iodo-2-propenoic

309   acid, 3-iodo-benzoic acid and 2-hydroxy-5-iodopyridine. I^-, I_3^- and iodide-organic adducts were quantified using KI

310   as surrogate standard by assuming their ionization efficiencies are similar in ESI- mode. The peak area of

311   iodide-organic adducts was calculated as the total peak area of extracted ion chromatogram of m/z 126.9039 after

312   RT 1 min. Iodide-metal complexes like CuI_2^-, $Cu_2I_3^-$, ZnI_3^- and $CuI_2(HCN)(HCl)^-$, if present, were also quantified

313   using KI but counted as I^-. IO_3^-, IO_2^- and IO^- were quantified using KIO_3 by assuming iodate, iodite and hypoiodite

314   have similar ionization efficiencies. Iodoacetic acid and 3-iodo-2-propenoic acid were quantified with their

315   respective standards. The other 3 non-aromatic compounds diiodoacetic acid, iodo-methanesulfonic acid and

316   diiodomethane were quantified using surrogate standard iodoacetic acid. All CHO and CHNO compounds observed

317   in ESI- mode were quantified using 3-iodo-benzoic acid, because they have similar structure of a carboxyl or

318   phenol group attached to aromatic rings. All CHNO and CHN compounds observed in ESI+ mode was quantified

319   with 2-hydroxy-5-iodopyridine by assuming these aromatic or heterocyclic amines have similar ionization

320   efficiencies. Due to the low amounts of individual aromatic compounds, a total concentration of all aromatic iodine

321   compounds detected was presented for each sample. Field blanks were processed in the same way and subtracted

322   from the aerosol samples.

323   There are a few weaknesses in the above-mentioned strategy. First, the use of surrogate standards can only be

324   regarded as semi-quantification for unassigned species. Second, there is still possibility that some unknown organic

325   iodine compounds are missed by our method shown in Figure 4. Third, inorganic iodine ions that elute around

326   0.5-0.7 min are prone to stronger matrix ion suppression effect than organic compounds. The underestimation may

327   be most serious if there are high concentration of co-eluting sulfate, nitrate and ammonium in the aerosol sample. A

328   linear regression analysis was conducted between the sum of all iodine species measured by this method and the

329   total iodine measured by ICP-MS. As shown in Figure 7, the total iodine concentration analyzed by our method is

330   90.5% on average of that obtained by ICP-MS with a correlation coefficient (R^2) 0.942. In spite of the above

331   uncertainties, our method provided a lower-limit estimate of iodine concentrations in ambient aerosols.

332   **3.3 Concentration and size distribution of iodine species during the NPF days at the coastal site**

333   We compared the total concentrations (Figure 8) and mass size distributions (Figure 9) of iodine species in 10

334   nm-18 μm particles during the I-NPF, continental NPF and non-NPF days at the coastal site. The particle number

335   size distributions during the same NPF days have been shown in Figure 2. It should be noted that, identical to

336   previous aerosol iodine speciation studies, the concentration reported here (pmol m^{-3}) is an average over the entire

337   3 sampling days. Thus, iodine concentrations during the intense NPF periods should be higher than the values

338   reported in this work. Continuous mass size distribution was fitted from the measured size-segregated mass

339   concentration data by assuming multimodal lognormal size distributions (Yu et al. 2010). Size distribution of

340   sulfate (HSO_4^-) was also shown (μg m^{-3}) in Figure 9. Because relative distribution in different sizes is not affected

341   by the uncertainties of semi-quantification, the size distributions are reported here with high confidence.

342   The highest total iodine concentration 126.3 pmol m^{-3} was found during the I-NPF days, which was 3.1 and

343   5.5 times higher than those during the continental NPF and non-NPF events, respectively. As shown in Figure 9a,

344   all iodine species except iodoacetic acid were characterized by a nucleation mode with mode diameters between

345   22-35 nm during the I-NPF days. This clearly shows that iodine was the NPF precursor in this type of NPF event.

346   The most remarkable iodine species during the I-NPF days is IO_3^- with a mole fraction of 42.5%. This is consistent

347   with the recent observation that HIO_3 is the key nucleating precursor in I-NPF event (Sipilä et al., 2016). On the

348   other hand, the sum of iodide ($[I^-]+[I_3^-]$) and iodide-organic adducts accounted for ~50 % of total iodine in newly

349   formed iodine particles. The presence of high iodide in clusters or new particles has not been reported by previous

350   field or laboratory measurements using CI-Api-TOF or AMS (O'Dowd et al., 2002; Mcfiggans et al., 2004; Sipilä

351   et al., 2016). Iodide is most likely from the partitioning of gaseous precursor HI formed during the photolysis of I_2

352   or iodomethane. HI itself is not a good nucleation precursor due to the lack of H-bond or halogen bond, but our

353   measurement suggests that HI might contribute to new particle growth in the size range as small as 10-18 nm. The

354   finding of HSO_4^- in nucleation mode is also interesting (Figure 6 and 9a), indicating that sulfuric acid also

355   contributed to new particle growth during the I-NPF days.

356   Although organic iodine compounds were most frequently found in the I-NPF samples (Table 1), they

357   accounted for only 6.8% of total iodine in the newly formed iodine particles. Considering the short lifetime of new

358   particles in the atmosphere, they were most likely from the heterogeneous uptake of gaseous HOI (formation route:

359   I →IO →HOI) and subsequent reactions with organics in the new particles. One exception is iodoacetic acid that

360   was characterized by a smaller accumulation mode and a larger coarse mode. Backward trajectory analysis showed

361   that air masses moved along the coast from the north during the I-NPF days. The unique size distribution of

362   iodoacetic acid indicates that direct sea salt emission was probably its major source.

363   Lower iodine concentrations during the continental NPF days and non-NPF days might be due to relatively

364   low iodine emission rate or transformation rate (from gaseous emission to particles) in non-algae growth season or

365   cloudy days. Iodine during the continental NPF days was characterized by an accumulation mode with mode

366   diameters between 500-700 nm (Figure 9b), except that iodoacetic acid had a coarse mode and 3-iodo-2-propenoic

367   acid had a 60 nm Aitken mode. Despite different size distribution from I-NPF, the mole fraction of iodide and

368   iodide-organic adducts were again ~50% of total iodine during the continental NPF. The outstanding species in the

369   continental NPF days were aromatic iodine compounds that accounted for 30% of total iodine. This is not

370   surprising because air masses from inland area of China on these days might contain a large amount of

371   anthropogenic aromatic substances. The predominance of accumulation mode implies that iodine was unlikely an

372   important nucleating precursor in the continental NPF. Direct uptake of gaseous HI or HOI onto

373   accumulation-mode aerosols seems also unlikely, because otherwise iodine should also be present in accumulation

374   mode during the I-NPF days. It is hypothesized that iodine species in the accumulation mode during the continental

375   NPF days were from the aging process of small iodine-containing particles. During the aging process, the organic

376   iodine compounds were formed from aqueous phase reactions between I^-, H_2O_2/O_3 and aromatic compounds via

377   in-cloud processing.

378   Iodoacetic acid and 3-iodo-2-propenoic acid surprisingly accounted for 44.3% of total iodine concentration

379   (22.8 pmol m^{-3}) during the non-NPF days. The high iodoacetic acid concentration, together with its presence in

380   coarse mode, again suggests its unique source associated with sea salt emission. 3-iodo-2-propenoic acid during

381   the non-NPF days and continental NPF days was characterized by a bimodal distribution with mode diameters

382   around 1 μm and 50-63 nm. In contrast, the bimodal distribution was replaced by a single small nucleation mode

383   during the I-NPF days. The sources of 3-iodo-2-propenoic acid and iodoacetic acid became more important during

384   the non-NPF days and merit more future investigation.

3.4 Comparison between coastal site and inland site

Table 2 gives a comparative overview of iodine species in $PM_{2.5}$ between the inland urban site and the coastal

site. The coastal samples include the 3 sets of nano-MOUDI data presented in Figure 8, from which the

concentrations of various iodine species in 10 nm - 3.2 μm particles were extracted to approximate $PM_{2.5}$; the rest

data were acquired by directly analysing the real $PM_{2.5}$ samples. It is found that total iodine was in the range of

6.5-11.2 and 19.5-122.6 pmol m^{-3} at the inland and coastal sites, respectively. Larger variation of iodine

concentrations at the coastal site is due to the inclusion of both I-NPF and non-NPF samples. The concentrations of

nearly all iodine species at the inland site were lower than those at the coastal site. This indicates that there were no

or relatively weak iodine emission sources surrounding the inland site. Our total iodine concentrations are in the

same order of magnitude as those reported at Mace Head (Gilfedder et al., 2008), an Ireland coastal site where

iodine NPF has long been reported, and Regensburg, an inland site of southern Germany (Wimschneider and

Heumann, 1995), although their maximum values are higher than ours.

Negligible amount of iodate (1.1%) was detected in only 1 out of the 4 inland samples. In fact, the

concentration of iodate was also low on the days without I-NPF events at the coastal site (on average 7±1%).

Therefore, iodate is a predominant species only in newly formed particles (Figure 9) and its concentration might be

reduced soon in the aging process via reactions like $IO_3^-+I^-+6H^+ \rightarrow 3I_2+3H_2O$ (Pechtl et al., 2007). The mole

fractions of iodide were 22.8±9.0% and 30.6±13.8% at the inland and coastal sites, respectively. Following the old

definition, the iodine species other than I- and IO_3^- were calculated as soluble organic iodine (SOI). Our finding is

that newly formed iodine particles were mostly composed of inorganic I^- and IO_3^- (68±20 % of the total iodine), but

SOI fraction increased to account for on average 76.3±6.9% of total iodine in the aged particles. Among the SOI

species, the largest fraction 63.7±7.7% was attributed to iodide-organic adducts at the inland site, followed by

aromatic iodine (11.5±2.8%) and iodoacetic acid (1.6±1.0%). All other species were not detectable or of negligible

407   amounts.

408   Table 2 clearly shows that more information on the speciation of soluble organic iodine in the aerosol samples

409   is provided in this study as compared to previous studies. In particular, a portion of iodine technically defined as

410   iodide-organic adducts was reported in our study for the first time, because they cannot survive in electrospray

411   ionization process even in most gentle source conditions, due to the weak bounding strength of I^- with organics.

412   I-organic adducts accounted for 63.7 ± 7.7 % in the inland urban samples and 30.8 ± 15.8% in the coastal samples.

413   Using IC-ICP-MS method, this portion of iodine is likely counted into organic iodine compounds. Our analysis

414   shows that this portion of iodine adducts can be attributed to neither stable organic iodine compounds nor free I^- ion.

415   Under certain condition, e.g., pH value, iodide-organic adducts probably release free I^- ion in the ambient aerosols.

416   **4. Conclusion**

417   Intense new particle formation events were observed during the algae growth and farming season at

418   Xianghshan Gulf, a coastal algaculture area of China. The high iodine concentration in nucleation mode particles

419   measured by UPLC/Q-TOF-MS confirmed that the NPF events were induced by iodine species. This is the first

420   study to investigate iodine-induced NPF in a place other than the coast sites of west Europe, Tasmania and Polar

421   regions. It is known that China produces more than 90 % seaweed of the world (1.5 million tons per year). Iodine is

422   likely emitted to the atmosphere and transformed to nano particles during the farming, harvesting and processing of

423   cultivated seaweed. Growing algae population due to serious eutrophication in the coastal waters of China also

424   promotes iodine emission. Therefore, farmed microalgae, as well as wild algae, could be an important source of

425   new particle formation in the coastal areas of China.

426   Using UPLC/Q-TOF-MS, inorganic I^-, IO_x^- and I_3^- were easily identified according to their accurate ion mass.

427   A large portion of iodide was observed to exist as weakly bound iodide-organic adducts. A signal amplification

428   approach was applied to look for organic iodine compounds, i.e., the compounds with C-I bond. For the first time,

429   35 molecular formulas, or 45 organic compounds according to the number of isomer peaks, were identified in

430   ambient aerosols. Iodine species on the I-NPF days and continental NPF days were characterized by a nucleation

431   mode and an accumulation mode, respectively. For the first time, high concentration of I^- was observed in particles

432   as small as 10-18 nm, suggesting gaseous HI may contribute to new particle growth in the I-NPF events. Iodate was

433   a remarkable species in only newly formed particles and was reduced in the aging process. Newly formed iodine

434   particles were mostly composed of inorganic I^- and IO_3^-, but SOI ([total iodine]-[I^-]-[IO_3^-]) accounted for the

435   majority of iodine in the aged particles. Generally speaking, organic iodine compounds resided in the same particle

436   mode as inorganic iodide. The exceptional coarse mode of iodoacetic acid indicates that direct sea salt emission

437   was probably its major source. During the continental NPF days, the characteristic iodine species is aromatic iodine

438   compounds that accounted for 30% of total iodine. Those aromatic iodine compounds were probably formed from

439   aqueous phase reactions between I^-, H_2O_2/O_3 and aromatic organic compounds during in-cloud processing.

440   Our study provided important information of iodine speciation, concentration and its role in NPF in the

441   context of heavy air pollution in eastern China. However, source, gas-particle partitioning and formation

442   mechanism of these iodine species are largely speculative. Moreover, the chemical composition and the role of

443   iodine in cluster sizes (1-3 nm) are still unknown. Simultaneous measurement of gaseous iodine precursors like I_2,

444   HI, HIO_x and IO_x using online instruments like CI-Api-TOF and DOAS are needed to elucidate the above questions.

445   On the other hand, more field measurements at multiple sites are required to test on what spatial scale iodine NPF

446   might be of relevance, in competition with other NPF precursors.

447   **ACKNOWLEDGMENTS**

448   The authors would like to thank the National Key Research and Development Program of China

449   (2016YFC0203100), the National Science Foundation of China (grant numbers. 41675124) and Jiangsu Specially

450   Appointed Professor Grant.

451   **References**

452   Allan, J.D., Williams, P.I., Najera, J., Whitehead, J.D., Flynn, M.J., Taylor, J.W., Liu, D., Darbyshire, E.,

453   Carpenter, L.J., Chance, R., Andrews, S.J., Hackenberg, S.C., McFiggans, G.: Iodine observed in new particle

454   formation events in the Arctic atmosphere during ACCACIA, Atmos. Chem. Phys., 15, 5599-5609, doi:

455   10.5194/acp-15-5599-2015, 2015.

456   Baker, A.: Marine aerosol iodine chemistry: The importance of soluble organic iodine, Environ. Chem., 2,

457   295-298, doi: 10.1071/EN05070, 2005.

458   Baker, A.R.: Inorganic iodine speciation in tropical Atlantic aerosol, Geophys. Res. Lett., 31, 187-206,

459   doi:10.1029/2004GL020144, 2004.

460   Baker, A.R., Sj, C.M.P., Jickells, T.D., Thompson, D.: Iodine concentration and availability in atmospheric

461   aerosol, Atmos. Environ., 34, 4331-4336, doi: 10.1016/s1352-2310(00)00208-9, 2000.

462   Baker, A.R., Tunnicliffe, C., Jickells, T.D.: Iodine speciation and deposition fluxes from the marine atmosphere,

463   J. Geophys. Res-Atmos., 106, 28743-28749, doi: 10.1029/2000JD000004, 2001.

464   Burkholder, J., Curtius, J., Ravishankara, A., Lovejoy, E.: Laboratory studies of the homogeneous nucleation of

465   iodine oxides, Atmos. Chem. Phys., 4, 19-34, doi: 1680-7324/acp/2004-4-19, 2004.

466   Chen, Z.L., Megharaj, M., Naidu, R.: Speciation of iodate and iodide in seawater by non-suppressed ion

467   chromatography with inductively coupled plasma mass spectrometry, Talanta, 72, 1842-1846, doi:10.

468   1016/j.talanta.2007.02.014, 2007.

469   Dai, L., Wang, H., Zhou, L., An, J., Tang, L., Lu, C., Yan, W., Liu, R., Kong, S., Chen, M.J.: Regional and local

470   new particle formation events observed in the Yangtze River Delta region, China: Simultaneous NPF

471   measurementsat 2 sites, J Geophys. Res-atmos., 122(4):2389-2402, doi: 10.1002 /2016JD026030, 2017.

472   Dall'Osto, M., Simo, R., Harrison, R. M., Beddows, D. C. S., Saiz-Lopez, A., Lange, R.,Skov, H., Nøjgaard, J.

473   K., Nielsen, I. E., and Massling, A.: Abiotic and biotic sources influencing spring new particle formation in North

474   East Greenland, Atmos. Environ., 190, 126-34, doi:10.1016/j.atmosenv.2018.07.019, 2018.

475   Ding, G., Zhang, X.: A picture of polar iodinated disinfection byproducts in drinking water by

476   (UPLC/)ESI-tqMS,Environ. Sci. Technol., 43, 9287, doi:10.1021/es901821a, 2009.

477   Dixneuf, S., Ruth, A.A., Vaughan, S., Varma, R.M., Orphal, J.: The time dependence of molecular iodine

478   emission from Laminaria digitata, Atmos. Chem. Phys., 9,823-829, doi:10.5194/ acp-9-823-200 9, 2009.

479   Draxler R R, Rolph G D: HYSPLIT-hybrid single particle lagrangian integrated trajectory model 2003 (NOAA

480   Air Resources Laboratory: Silver Spring, MD) http://ready.arl.noaa.gov/HYSPLIT.php, 2003.

481   Gilfedder, B. S., Lai, S. C., Petri, M., Biester, H., Hoffmann, T.: Iodine speciation in rain, snow and aerosols,

482   Atmos. Chem.Phys., 8, 6069-6084, doi: 10.5194/acp-8-6069-2008, 2008.

483   Gilfedder, B.S., Petri, M., Beister, H.: Iodine Speciation in Rain and Snow, Nucl. Atmos. Aero., doi:

484   10.1007/978-1-4020-6475-3_108, 2007a.

485   Gilfedder, B.S., Petri, M., Biester, H.: Iodine speciation in rain and snow: Implications for the atmospheric

486   iodine sink, J. Geophys. Res-atmos.,112, doi:10.1029/2006JD007356, 2007b.

487   Grose, M.R., Cainey, J.M., McMinn, A., Gibson, J.A.E.: Coastal marine methyl iodide source and links to new

488   particle formation at Cape Grim during February 2006. Environ Chem 4, 172-177.doi: 10.1071/EN07008, 2007

489   Hughes, C., Malin, G., Nightingale, P.D., Liss, P.S.: The Effect of Light Stress on the Release of Volatile

490   Iodocarbons   by   Three   Species   of   Marine   Microalgae,Limnol.   Oceanogr.,   51,   2849-2854,

491   doi:10.4319/lo.2006.51.6.2849, 2006.

492   Kaňa, A., Hrubá, L., Vosmanská, M., Mestek, O.: Analysis of iodine and its species in animal tissues, Chemical.

493   Spec. Bioavailab., 27, 81-91, doi: 10.1080/09542299.2015.1087160, 2015.

494   Lai, S.C., Hoffmann, T., Xie, Z.Q.: Iodine speciation in marine aerosols along a 30,000 km round‑trip cruise

495   path from Shanghai, China to Prydz Bay, Antarctica, Geophys. Res. Lett., 35, L21803, doi:10.1029/2008gl035492,

496   2008.

497   Lee, B. H., Lopez-Hilfiker, F. D., Mohr, C., Kurtén, T., Worsnop, D. R., and Thornton, J. A.: An Iodide-Adduct

498   High-Resolution Time-of-Flight Chemical-Ionization Mass Spectrometer: Application to Atmospheric Inorganic

499   and Organic Compounds, Environ. Sci. Technol., 48(11).48,6309-6317, doi:10.1021/es5003 62a, 2014.

500   Liu, W., Yang, H., Li, B., Xu, S.: Determination of Bromine and Iodine Speciation in Drinking Water Using

501   High Performance Liquid Chromatography‑Inductively Coupled Plasma‑Mass Spectrometry, Geostand.

502   Geoanal. Res, 35, 69-74., doi:10.1111/j.1751-908X.2010.00033.x, 2015.

503   Mahajan, A.S., Sorribas, M., Gómez Martín, J.C., MacDonald, S.M., Gil, M., Plane, J.M.C., Saiz-Lopez, A.:

504   Concurrent observations of atomic iodine, molecular iodine and ultrafine particles in a coastal environment, Atmos.

505   Chem. Phys.,11, 2545-2555, doi: 10.5194/acp-11-2545-2011, 2011.

506   Martín, J.C., Gómez, Gálvez, O., Baeza-Romero, M.T., Ingham, T., Plane, J.M.C., Blitz, M.A.: On the

507   mechanism of iodine oxide particle formation, Phys. Chem. Chem. Phys., 15, 15612-15622,

508   doi:10.1039/c3cp51217g, 2013.

509   McFiggans, G., Bale, C. S. E., Ball, S. M., Beames, J. M., Bloss, W. J., Carpenter, L. J., Gallagher, M. W.:

510   Iodine-mediated coastal particle formation: an overview of the Reactive Halogens in the Marine Boundary Layer

511   (RHaMBLe) Roscoff coastal study, Atmos. Chem. Phys., 10,2975-2999, doi: 10.5194/acp-10-2975-2010, 2010.

512   Mcfiggans, G., Coe, H., Burgess, R., Allan, J., Cubison, M., Alfarra, M. R.: Physics Direct evidence for coastal

513   iodine particles from Laminaria macroalgae – linkage to emissions of molecular iodine, Atmos. Chem. Phys., 4,

514   701-713, doi: 10.5194/acp-4-701-2004, 2004.

515   O'Dowd, C. D., Kaarle, H., Jyrki, M., Minna, V., Pasi, A., Gerrit, D. L.: Coastal new particle formation:

516   Environmental conditions and aerosol physicochemical characteristics during nucleation bursts, J. Geophys.

517   Res-atmos., 107, PAR 12-11–PAR 12-17, doi:10.1029/2000JD000206, 2002.

518   O'Dowd,C.D., Jimenez, J.L., Bahreini, R.: Marine aerosol formation from biogenic iodine emissions, Nature,

519   417(6889):632-636, doi: 10.1038/nature00775, 2002.

520   O'Dowd, C. D., De Leeuw, G.: Marine aerosol production: a review of the current knowledge, Philos. T R Soc.

521   A., 365, 1753-1774, doi:10.1098/rsta.2007.2043, 2007.

522   Palmer, C.J., Anders, T.L., Carpenter, L.J., Küpper, F.C., Mcfiggans, G.B.: Iodine and halocarbon response of

523   laminaria digitata to oxidative stress and links to atmospheric new particle production, Environ. Chem., 2, 282-290,

524   doi:10.1071/EN05078, 2005.

525   Pechtl, S., Schmitz, G., von Glasow, R.: Modelling iodide–iodate speciation in atmospheric aerosol:

526   Contributions of inorganic and organic iodine chemistry, Atmos. Chem. Phys., 7, 1381-1393,

527   doi:10.5194/acp-7-1381-2007, 2007.

528   Redeker, K.R., Wang, N., Low, J.C., Mcmillan, A., Tyler, S.C., Cicerone, R.J.: Emissions of methyl halides and

529   methane from rice paddies, Science, 290, 966-969, doi:10.1126/science.290.5493.966, 2000.

530   Roscoe, H. K., Jones, A. E., Brough, N., Weller, R., Saiz-Lopez, A., Mahajan, A. S., Schoenhardt, A., Burrows,

531   J. P., and Fleming, Z. L.: Particles and iodine compounds in coastal Antarctica, J. Geophys. Res.-Atmos., 120,

532   7144-7156, doi:10.1002/2015JD023301, 2015.

533   Saiz-Lopez, A., Plane, J.M., Baker, A.R., Carpenter, L.J., Von, G.R., Mart ń, J.C., Mcfiggans, G., Saunders,

534   R.W.: Atmospheric chemistry of iodine, Chem. Rev., 112, 1773-1804, doi:10.1021/cr200 029u, 2012a.

535   Sellegri, K., Yoon, Y.J., Jennings, S.G., O'Dowd, C. D., Pirjola, L., Cautenet, S.: Quantification of coastal new

536   ultra-fine particles formation from in situ and chamber measurements during the BIOFLUX campaign, Environ.

537   Chem., 2, 260-270, doi:10.1071/EN05074, 2006.

538   Seto, F.Y.B., Duce, R.A.: A laboratory study of iodine enrichment on atmospheric sea-salt particles produced by

539   bubbles, J Geophy. Res., 77, 5339-5349 , doi:10.1029/JC077i027p05339, 1972.

540   Shah, M., Wuilloud, R.G., Kannamkumarath, S.S., Caruso, J.A.: Iodine speciation studies in commercially

541   available seaweed by coupling different chromatographic techniques with UV and ICP-MS detection, J Anal. Atom.

542   Spectrom., 20, 176-182, doi:10.1039/b415756g, 2005.

543   Sipilä, M., Sarnela, N., Jokinen, T., Henschel, H., Junninen, H., Kontkanen, J., Richters, S., Kangasluoma, J.,

544   Franchin, A., Peräkylä, O.: Molecular-scale evidence of aerosol particle formation via sequential addition of HIO3,

545   Nature, 537, 532, doi:10.1038/nature19314, 2016.

546   Sive, B.C., Varner, R.K., Mao, H., Blake, D.R., Wingenter, O.W., Talbot, R.: A large terrestrial source of methyl

547   iodide, Geophy. Res. Lett., 34, 251-270 , doi:10.1029/2007gl030528, 2007.

548   Wang, K.E., Jiang, S.J.: Determination of iodine and bromine compounds by ion chromatography /dynamic

549   reaction cell inductively coupled plasma mass spectrometry, Anal. Sci., 24, 509-514 , doi:10.2116/analsci.24.509,

550   2008.

551   Wei, L., Hongxia, Y., Bing, L., Dengyun, C., Huijuan, Z.: Speciation Stabilities of Iodine in underground Water

552   by High Performance Liquid Chromatography-Inductively Coupled Plasma Mass Spectrometry, Chinese J of Anal.

553   Chem., 35, 571-573, doi: 10.1016/s1872-2040(07)60047-4, 2007.

554   Wimschneider, A., Heumann, K.G.: Iodine speciation in size fractionated atmospheric particles by isotope

555   dilution mass spectrometry, Fresen. J Anal. Chem., 353, 191-196, doi:10.1007/BF00322957, 1995.

556   Xu, S., Xie, Z., Li, B., Liu, W., Sun, L., Kang, H., Yang, H., Zhang, P.: Iodine speciation in marine aerosols

557   along a 15 000-km round-trip cruise path from Shanghai, China, to the Arctic Ocean, Enviro. Chem., 7, 406-412,

558   doi: 10.1071/EN10048, 2010.

559   Yang, Y., Peng, Y., Chang, Q., Dan, C., Guo, W., Wang, Y.: Selective Identification of Organic Iodine

560   Compounds Using Liquid Chromatography-High Resolution Mass Spectrometry, Anal. Chem.,88, 1275, doi:

561   10.1021/acs.analchem.5b03694, 2016.

562   Yoon, Y. J., O'Dowd, C. D., Jennings, S. G., Lee, S. H.: Statistical characteristics and predictability of particle

563   formation events at Mace Head, J Geophy. Res.111,doi:10.1029/2005JD00 6284, 2006.

564   Yoshida, S., Muramatsu, Y., Katou, S., Sekimoto, H.: Determination of the chemical forms of iodine with

565   IC-ICP-MS and its application to environmental samples, J Radioanal. Nucl. Chem., 273, 211-214,

566   doi:10.1007/s10967-007-0738-4, 2007.

567   Yu, H. , Zhou, L., Dai, L., Shen, W., Dai, W., Zheng, J.: Nucleation and growth of sub-3 nm particles in the

568   polluted urban atmosphere of a megacity in China, Atmos. Chem. Phys., 16, 18653-18690,

569   doi:10.5194/acp-16-2641-2016, 2016.

570   Yu, H., Wu, C., Wu, D., Yu, J. Z.: Size Distributions of Elemental Carbon and its Contribution to Light

571   Extinction in Urban and Rural Locations in the Pearl River Delta region, China, Atmos. Chem. Phys., 10:

572   5107-5119, doi:10.5194/acp-10-5107-2010, 2010.

573   Yun, L., Peng, Y., Chang, Q., Zhu, Q., Guo, W., Wang, Y.: Identification of Organic Iodine Compounds and their

574   Transformation Products in Edible Iodized Salt using Liquid Chromatography-High Resolution Mass Spectrometry,

575   J Agr. Food Chem., 65, 5384-5389, doi:10.1021/acs.jafc.7b01759, 2017.

576   Zhang, X.: A picture of polar iodinated disinfection byproducts in drinking water by (UPLC/)ESI-tqMS,

577   Environ. Sci. Technol.,43, 9287., doi:10.1021/es901821a, 2009.

578   Zhang, W., Liu, X., Jia, X., Yi, H., Liu, X., Xie, X., Lu, J., Duan, T., Chen, H.: Fast Speciation of Iodide and

579   Iodate in Edible Salts and Human Urine by Short Column IC Coupled with Inductively Coupled Plasma MS,

580   Chromatographia., 72, 1009-1012, doi:10.1365/s10337-010-1756-x, 2010.

Table 1. Organic iodine compounds that were detected at least once in the aerosol samples. n: the number of samples. Four $PM_{2.5}$ samples were collected at the inland site; three $PM_{2.5}$ samples and three sets of nano-MOUDI samples were collected at the coastal site. m/n numbers in right 4 columns: a given molecular formula was detected in m out of n samples. A blank cell means the formula was not detected in any samples. Also shown are measured ion mass, exact ion mass and the number of isomers based on the number of chromatographic peaks observed for given ion mass in the samples. Bold formulas are observed in ESI+ mode and others in ESI- mode.

Molecular formula	Measured ion mass (Da)	exact ion mass (Da)	Isomer number	Coastal site (n=6)			Inland site (n=4)	All samples
				I-NPF	Continental NPF	Non-NPF		
$C_2H_3O_2I$	184.9099	184.9099	1	3/4	1/1	1/1	4/4	9/10
$C_3H_3O_2I$	196.9098	196.9099	1	4/4	1/1		1/4	6/10
CH_2I_2	266.8177	266.8168	1	3/4	1/1		1/4	5/10
$C_2H_2O_2I_2$	310.8079	310.8066	1	4/4				4/10
$CH_2SO_3I_2$	346.7743	346.7736	1	2/4	1/1			3/10
$C_6H_4NO_4I$	279.9112	279.9107	1	3/4	1/1	1/1	4/4	9/10
$C_{10}H_6NO_3I$	313.9319	313.9314	1	4/4	1/1	1/1	3/4	9/10
$C_6H_4NO_3I$	263.9164	263.9158	1	4/4	1/1	1/1	2/4	8/10
$C_7H_6NO_4I$	293.9269	293.9263	2	3/4	1/1			4/10
$\mathbf{C_5H_4NOI}$	221.9414	221.9416	2	3/4				3/10
$\mathbf{C_6H_6NOI}$	235.9571	235.9572	2	3/4				3/10
$\mathbf{C_7H_8NOI}$	249.9726	249.9729	3	3/4				3/10
$C_9H_{10}NO_4I$	321.9572	321.9576	2	1/4	1/1		1/4	3/10
$C_8H_6NO_5I$	321.9216	321.9212	1	2/4				2/10
$\mathbf{C_9H_6NOI}$	271.9570	271.9572	2	2/4				2/10
$C_8H_8NO_5I$	323.9370	323.9369	1	1/4				1/10
$C_8H_7O_2I$	260.9411	260.9412	1	3/4	1/1	1/1	2/4	7/10
$C_7H_5O_4I$	278.9156	278.9154	2	2/4	1/1	1/1	2/4	6/10
$C_7H_5O_2I$	246.9260	246.9256	1	3/4	1/1		1/4	5/10
$C_8H_5O_3I$	274.9210	274.9205	1		1/1		2/4	3/10
$C_6H_3OI_3$	470.7245	470.7240	1	1/4	1/1			2/10
$C_7H_4O_3I_2$	388.8177	388.8172	1	1/4	1/1			2/10
$C_7H_5O_3I$	262.9209	262.9205	2	1/4	1/1			2/10
$C_7H_6O_2I_2$	374.8383	374.8379	1	1/4	1/1			2/10
$C_7H_7O_4I$	280.9298	280.9311	1	2/4				2/10
$C_8H_4O_2I_2$	372.8230	372.8222	1	1/4	1/1			2/10
$C_8H_6O_2I_2$	386.8382	386.8379	1	1/4	1/1			2/10
$C_8H_6O_3I_2$	402.8319	402.8328	1	1/4	1/1			2/10
$C_8H_7O_3I$	276.9361	276.9362	1	1/4	1/1			2/10
$C_8H_8O_3I_2$	404.8489	404.8485	1	2/4				2/10
$C_9H_7O_3I$	288.9372	288.9362	1	1/4				1/10
$C_9H_7O_4I$	304.9309	304.9311	2	1/4				1/10
$\mathbf{C_7H_{11}N_2I}$	251.0044	251.0045	1	3/4			1/4	4/10
$\mathbf{C_8H_{11}N_6I}$	319.0172	319.0168	1	1/4				1/10

$C_4H_4N_2I_2$	334.8547	334.8542	1	1/1	1/10

Table 2. Comparison of iodine species in $PM_{2.5}$ between the inland urban site and the coastal site. iodide: the sum of I^-, I_3^- and I^--metal complexes (if present). IO_x^-: the sum of IO_3^-, IO_2^- and IO^-; SOI: soluble organic iodine that is calculated as the difference between total iodine and the sum of iodide and IO_x^-. I-AA: the sum of iodoacetic acid and diiodoacetic acid; I-PA: iodopropenoic acid; I-MSA: iodomethanesulfonic acid; CHI_2^-: diiodomethane; I-aromatics: total aromatic iodine compounds; I^--organic adducts: iodide-organic adducts. Also shown are iodine species measured by IC-ICP-MS at Mace Head (Gilfedder et al., 2008), an Ireland coastal site, and Regensburg (Wimschneider and Heumann, 1995), an inland site of southern Germany.

Iodine species	Inland site (n=4)		Coastal site (n=6)		Mace Head, Ireland		Regensburg, Germany	
	Conc. (pmol m^{-3})	%	Conc. (pmol m^{-3})	%	Conc. (pmol m^{-3})	%	Conc (pmol m^{-3})	%
iodide	1.0-3.7	22.8±9.0	3.8-74.1	30.6±13.8	0.3-58	3.7-30	3.1-7.2	12-31
IO_x^-	ND-0.087	0.3±0.6	1.5-53.1	23.1±14.0	nd-15	0.1-7.2	12.6-54.2	69-88
SOI	5.4-7.5	76.9±8.6	14.2-66.1	46.3±27.3	3.7-509	69-96		
I^--organic adducts	4.3-6.1	63.7±7.7	6.7-62.9	30.8±15.8				
CH_2I^-	ND-0.083	0.2±0.4	0.036-0.74	0.4±0.7				
I-AA	0.054-0.25	1.6±1.0	0.57-2.2	4.8±5.6				
I-MSA	ND	0	ND-0.28	0.09±0.12				
I-PA	ND-0.016	0.04±0.07	0.16-5.2	5.9±4.6				
I-aromatics	0.76-1.2	11.5±2.8	0.1-12.3	6.7±6.8				
Total Iodine	6.5-11.2		19.5-122.6		10-532		15.7-61.3	

Figure 1. Locations of two sampling sites: ① the coastal site at Xiangshan Gulf ② the inland urban site that is 200 km from the coast. The blue color indicates the coastal area of China.
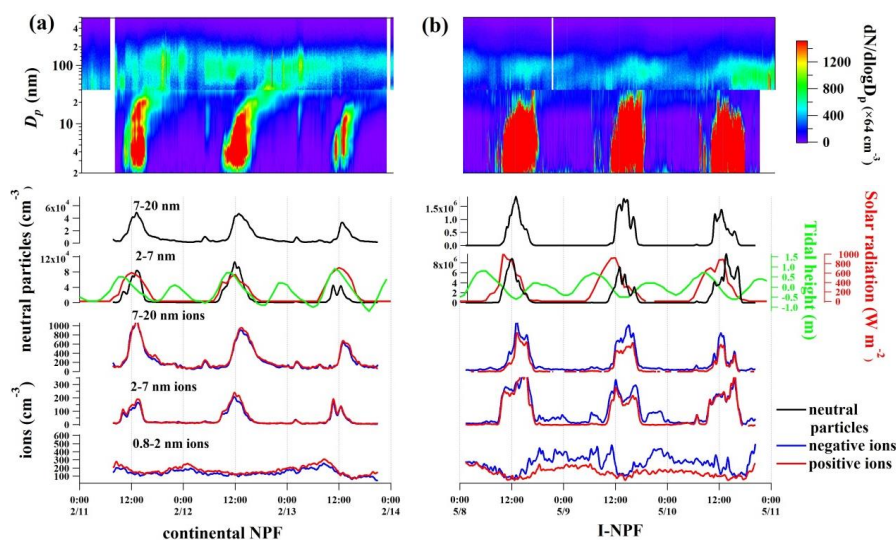
Figure 2. Particle number concentration during (a) the continental NPF days from February 11 to 13, 2018 and (b) the iodine-induced NPF (I-NPF) days from May 8 to 11, 2018. From top to bottom: particle size spectra of the NPF events; diurnal variations of 7-20 nm and 2-7 nm neutral particles (black curves); diurnal variations of 7-20 nm, 2-7 nm and 0.8-2 nm negative (blue curves) and positive ions (red curves). Solar radiation and tidal height were obtained from local maritime authority and plotted as red and green curves, respectively.
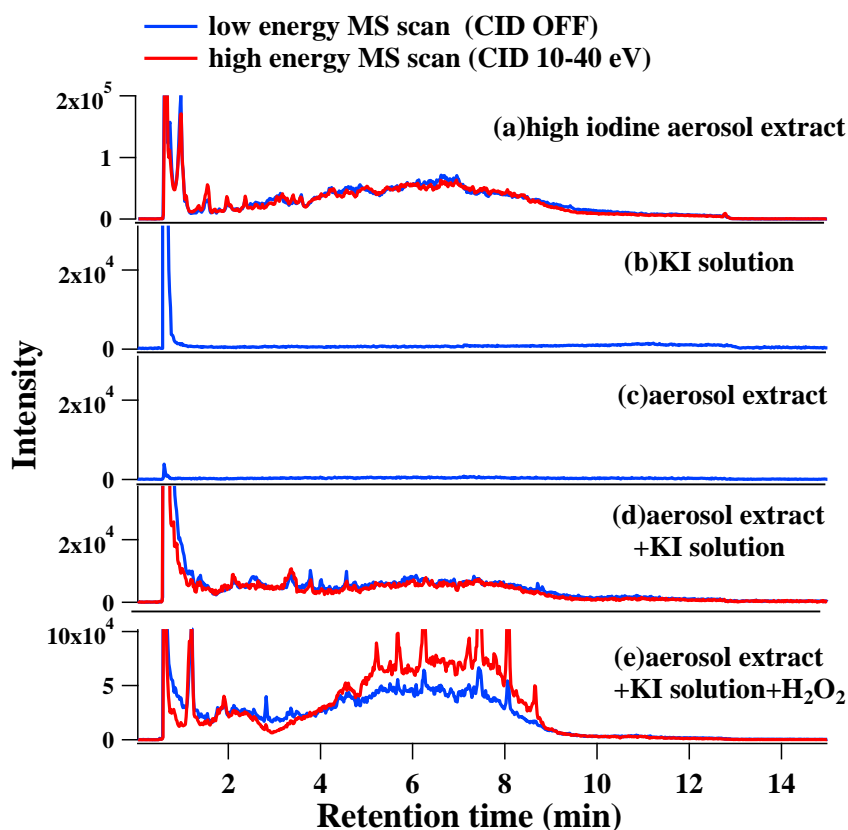
Figure 3. Ion chromatograms of m/z 126.9039 of (a) aerosol extract with high concentration of iodine, (b) pure potassium iodide (KI) solution (1 mmol L^{-1}), (c) aerosol extract with low concentration of iodine, (d) the KI solution mixed with the aerosol extract with low concentration of iodine and (e) The KI solution+aerosol extract mixture with the addition of 10 mmol L^{-1} H$_2$O$_2$ solution. Blue curves: low energy MS scan mode, in which collision induced dissociation is off and molecular ions are subject to in-source fragmentation only. Red curves: high energy MS scan mode, in which molecular ion are subject to both in-source fragmentation and 10-40 eV collision induced dissociation.

	Steps	MS method	Data acquired
1	MD *vs.* m/z diagram comparison between aerosol and aerosol+KI+H_2O_2/O_3	Low energy MS scan	m/z and RT of potential organic iodine ions
2	Elemental composition calculation Chemspider search	MSMS confirmation	80 possible CHONSI chemical formulas
3	Targeted screening in real aerosol samples based on m/z and RT	Low energy MS scan	35 formulas (47 organic iodine compounds) and their peak area observed in aerosol samples
4	4 compounds quantified with their standards; 43 compounds semi-quantified with surrogate standards	Low energy MS scan of commercial standards	Concentrations of individual non-aromatic compounds and total aromatic iodine compounds

Figure 4. Identification and semi-quantification steps of unknown organic iodine compounds in ambient aerosols
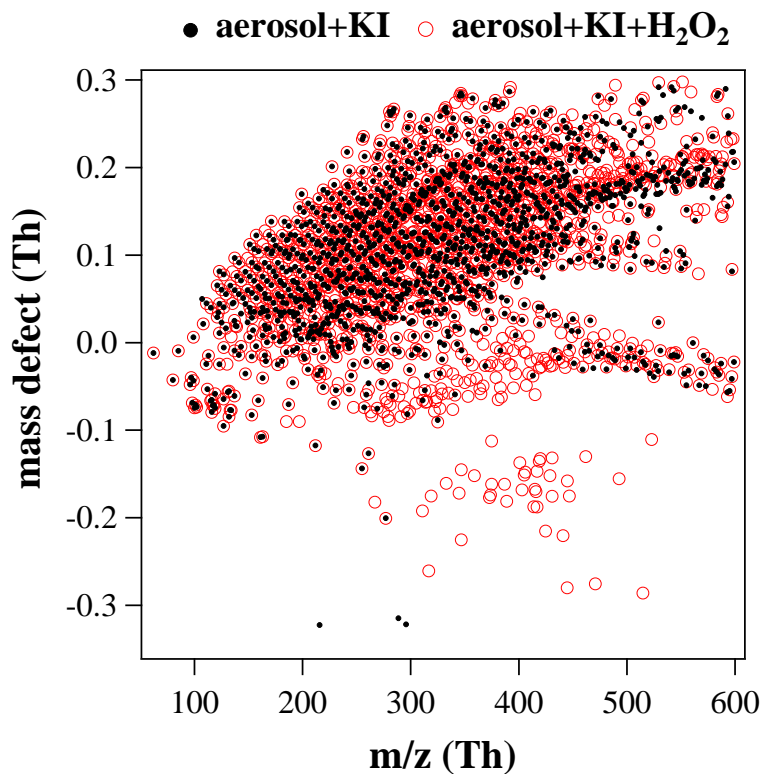
Figure 5. Mass defect (MD) *vs.* m/z diagram of molecular ions before (black dots) and after (red circles) the addition of H_2O_2 into aerosol extract+KI mixture. The mass spectrum of all ions above background level (10^4) was reconstructed by integrating over retention time 0-15 min.
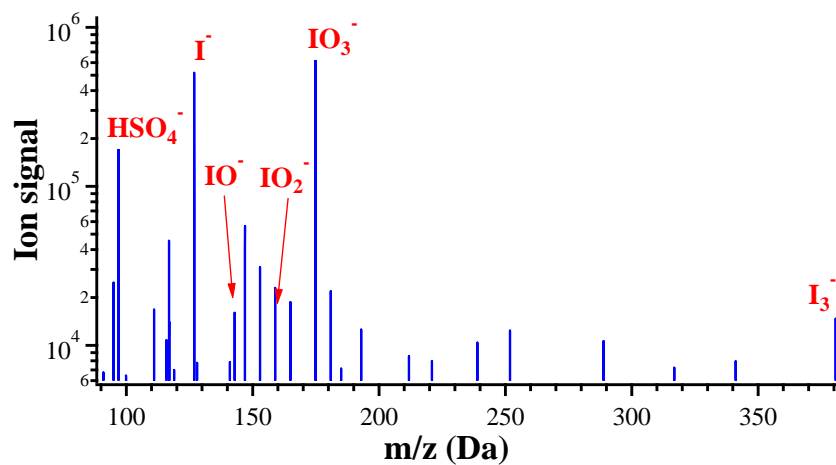
Figure 6. Integrated mass spectrum of molecular ions between retention time 0.5-0.7 min of an S13 nano-MOUDI sample (10-18 nm particles).
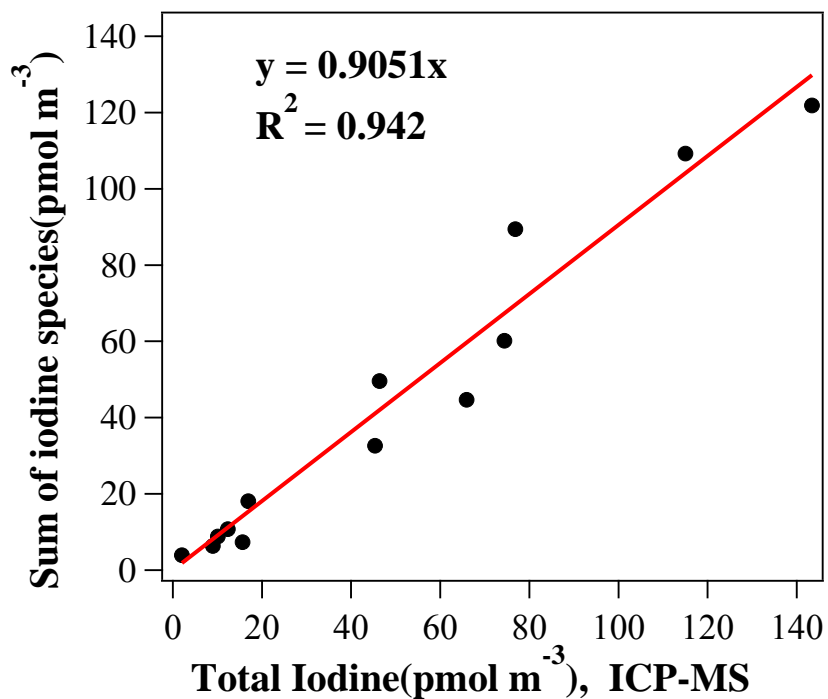
Figure 7. A comparison between the sum of all iodine species measured by our method and total iodine concentration measured by ICP-MS. Red line shows the linear regression between the two methods with a correlation coefficient R^2 0.942.
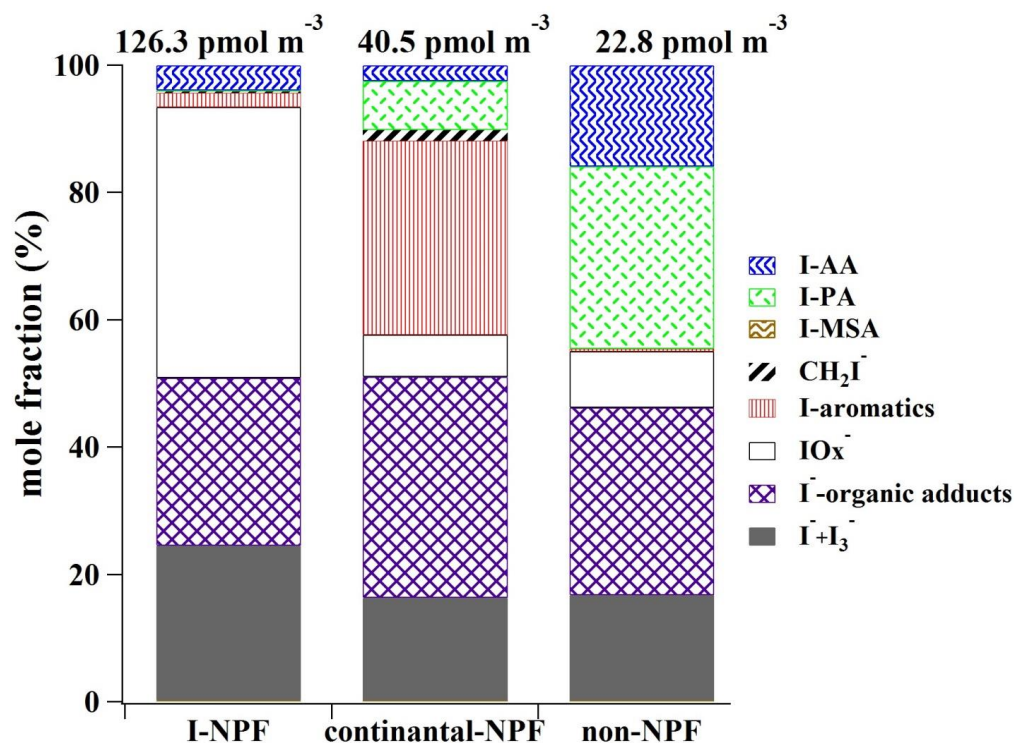
Figure 8. Total concentrations and mole fractions of iodine species in 10 nm-18 μm particles during the iodine-induced NPF (I-NPF), continental NPF and non-NPF days. I-AA: the sum of iodoacetic acid and diiodoacetic acid; I-PA: iodopropenoic acid; I-MSA: iodomethanesulfonic acid; CHI_2^-: diiodomethane; I-aromatics: total aromatic iodine compounds; IO_x^-: $[IO_3^-]+[IO_2^-]+[IO^-]$; I^--organic adducts: iodide-organic adducts; $I^-+I_3^-$: the sum of iodide and triiodide.
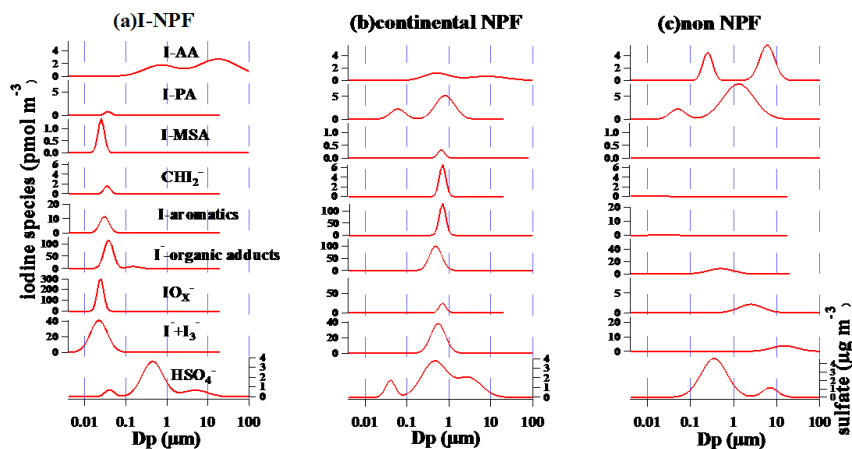
Figure 9. Mass size distribution of iodine species in 10 nm-18 µm particles during (a) iodine-induced NPF (I-NPF), (b) continental NPF and (c) non-NPF days. Continuous size distributions of iodine species were inverted from the measured mass concentrations in the 13 size bins of nano-MOUDI. I-AA: the sum of iodoacetic acid and diiodoacetic acid; I-PA: iodopropenoic acid; I-MSA: iodomethanesulfonic acid; CHI_2^-: diiodomethane; I-aromatics: total aromatic iodine compounds;IO_x^-: $[IO_3^-]+[IO_2^-]+[IO^-]$; I$^-$-organic adducts:iodide-organic adducts; $I^-+I_3^-$: the sum of iodide and triiodide